

Online Appendix Material and Methods: Pancreatic RNA isolation and quantitative real-time (q)RT-PCR. Mice were fasted overnight and killed 1 hour (h) after feeding. A small slice (~5-10 mm³) was taken from a transverse section of the pancreatic tail (adjacent to the spleen), and immediately homogenized in Trizol (Invitrogen) using a stainless steel generator probe (Omni International, Marietta, GA). RNA was purified by standard chloroform extraction technique, and RNA integrity was verified for each sample by 1% agarose gel electrophoresis, and Agilent 2100 Bioanalyzer (Agilent Technologies, Santa Clara, CA). While isolation of rodent pancreatic RNA often is difficult, in our hands, this approach virtually always produced good quality RNA. We found that feeding the mice immediately before obtaining the pancreatic tissue sample, and prompt tissue processing to be most important to prevent pancreatic RNA degradation. RNA was also prepared from purified islets and islet-depleted cells of individual mice by Trizol homogenization and chloroform extraction. 1 µg of total RNA was reverse transcribed into cDNA using the 1st Strand Synthesis Kit by random priming. Real time quantitative PCR reactions were run on an ABI Prism 7700 Sequence Detector (Applied Biosystems, Foster City, CA). Hormone gene expression was tested using the following murine primer-probe sets from Applied Biosystems: Ins (Mm00731595_gH), Gcg (Mm00801712_m1), Sst (Mm00436671_m1), and Ppy (Mm00435889_m1), and 18s RNA (4319413E). Reactions were run at least twice.

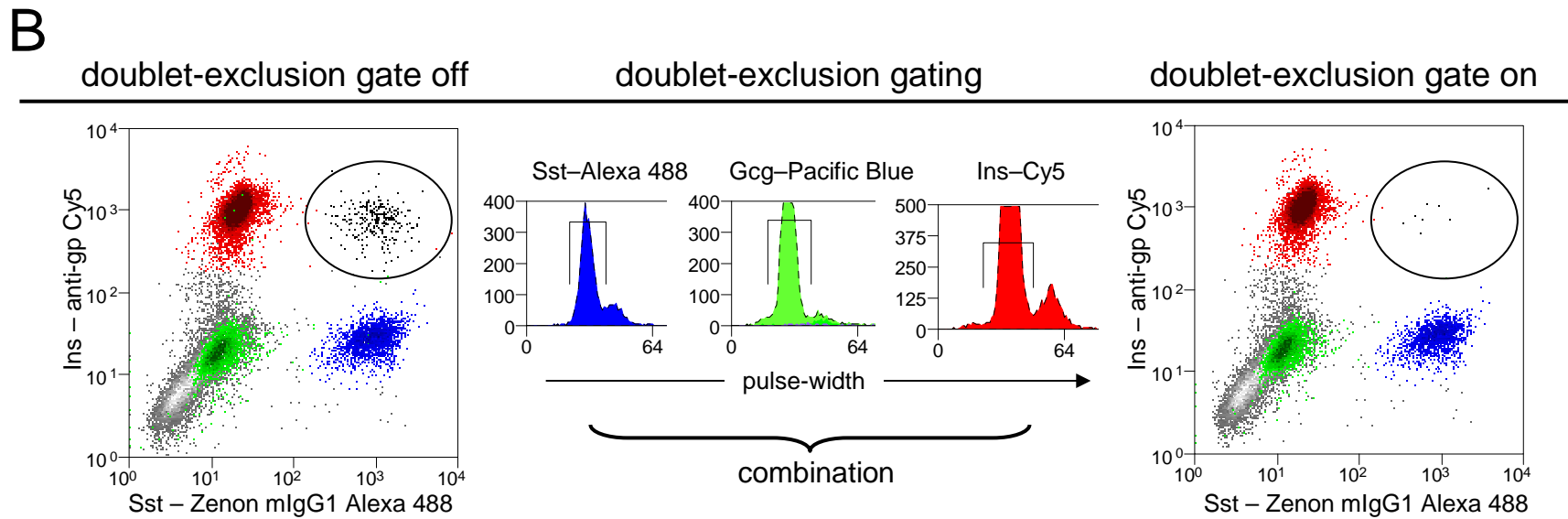
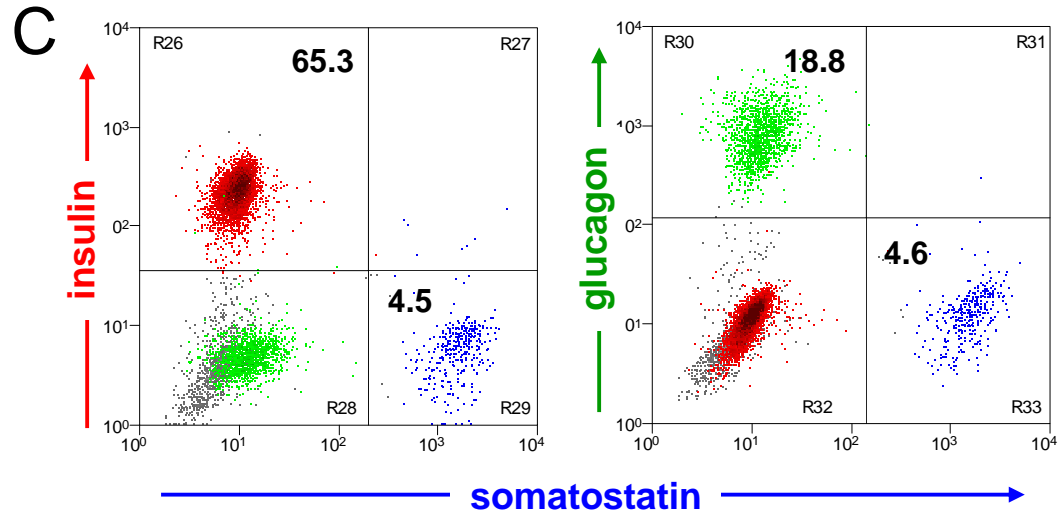
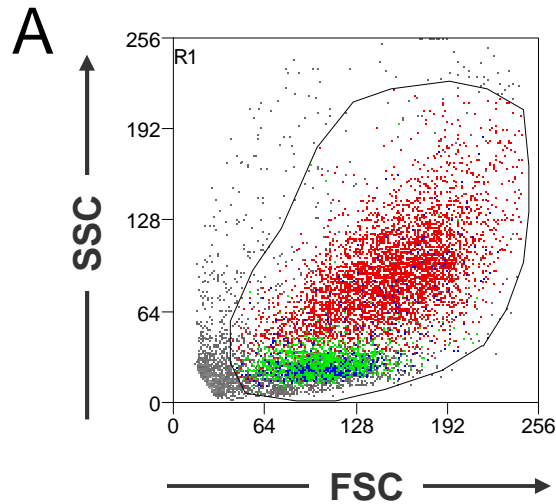
Online Appendix Table 1 Pechhold et al.

Online Appendix Table 1: quantitative Analysis of naïve and recently diabetic pancreas by confocal fluorescence microscopy

Mouse	Diabetes		Islet Size HSIC (median)	HSIC scored				
	onset	duration		total	insulin ⁺ (%)	glucagon ⁺ (%)	somatostatin ⁺ (%)	ins+/gln+ (ratio)
	(days)							
<u>C57BL/6</u>								
1	naïve		39	903	78	19	3	4.0 ^a
2	naïve		44	1063	76	19	5	4.0
3	naïve		14	142	77	13	10	5.8
<u>Rip-CD80+GP+</u>								
1	naïve		27	748	66	26	8	2.6 ^b
2	naïve		9	192	82	14	4	5.9
3	naïve		7	677	82	13	4	6.1
<u>chronic progression</u>								
4	55	1	15	333	30	49	21	0.6 ^c
5	36	0	24	660	35	46	20	0.8
6	44	1	13	863	45	38	17	1.2
7	50	4	8	312	59	31	11	1.9
8	51	1	10	580	64	22	14	2.9
9	48	2	32	427	84	13	3	6.4
10	40	0	21	1071	81	12	7	6.7
11	55	1	12	640	82	11	7	7.6
12	60	1	12	220	85	8	8	10.9

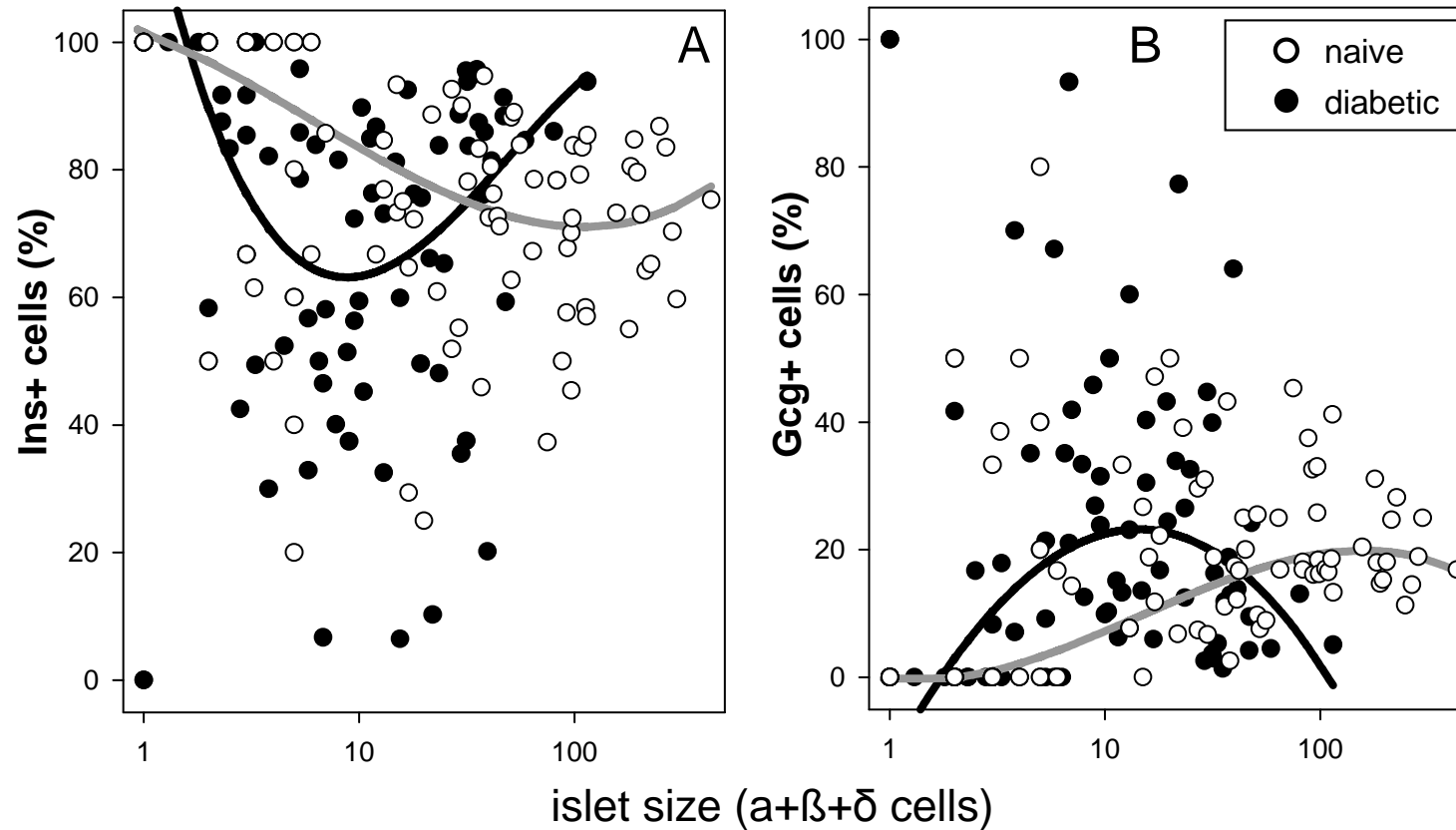
Mean±S.D. of Ins+ to Gcg+ ratios of groups of mice: (a) 4.6±1.0; (b) 4.9±1.6; (c) 4.3±3.5;

Online Appendix Figure 1 Pechhold et al.



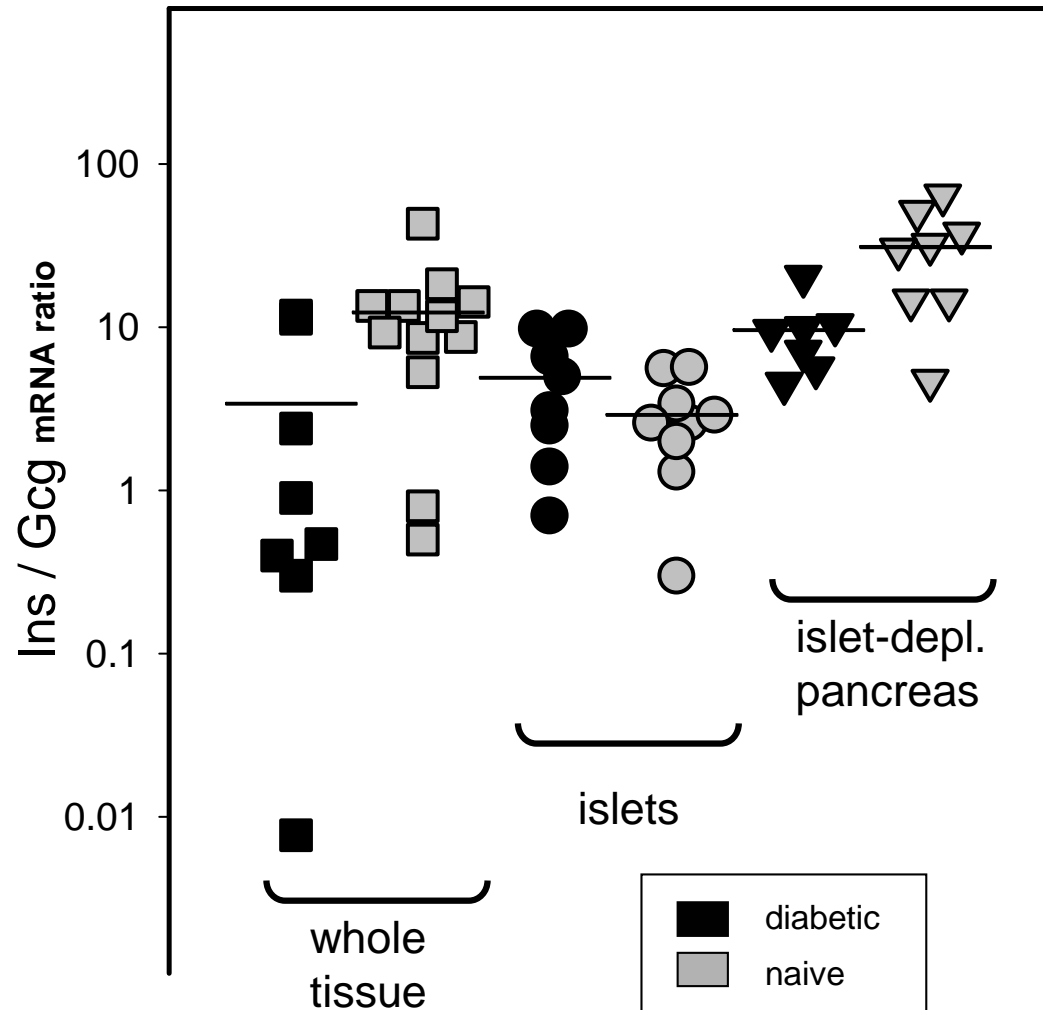
Online Appendix Figure 1: Complete gating strategy and analysis of C57BL/6 dissociated islet cells, corresponding to Figure 1B. A, electronic light scatter gates applied to dissociated, intracytoplasmically stained islet cells. Colors indicate the characteristic forward and sideward light scatter patterns found in the major endocrine subsets of healthy mice (see also Figure 2). B, electronic doublet exclusion gating strategy using pulse width discrimination facilitates the exclusion of islet cells not dissociated into a single cell suspension. The technique exploits the principle of hydrodynamic focusing, the focused flow of sample and sheath fluid which ensures that cells line up as they pass through the nozzle in the flow cell where they intersect the laser beam. An pulse width increased by a factor of approx. 2 occurs if two similar events cannot be differentiated by laser detection because they are too close (e.g. doublets). Seemingly Ins+Sst+ double positive cells (B, lower left dot plot, circled population) are entirely contained in the increased pulse width subset. Combination gating on endocrine islet cell subsets with single-cell pulse width eliminated the Ins+Sst+ double-positive population (B, right dot plot, circle). In our hands, pulse width-based doublet exclusion eliminated more than 96% of doublets regularly present after incomplete dissociation of pancreatic islets. C, Resulting two-dimensional displays of combinations and frequencies of the major endocrine cell frequencies is shown (complementing results of Figure 1B).

Online Appendix Figure 2 Pechhold et al.



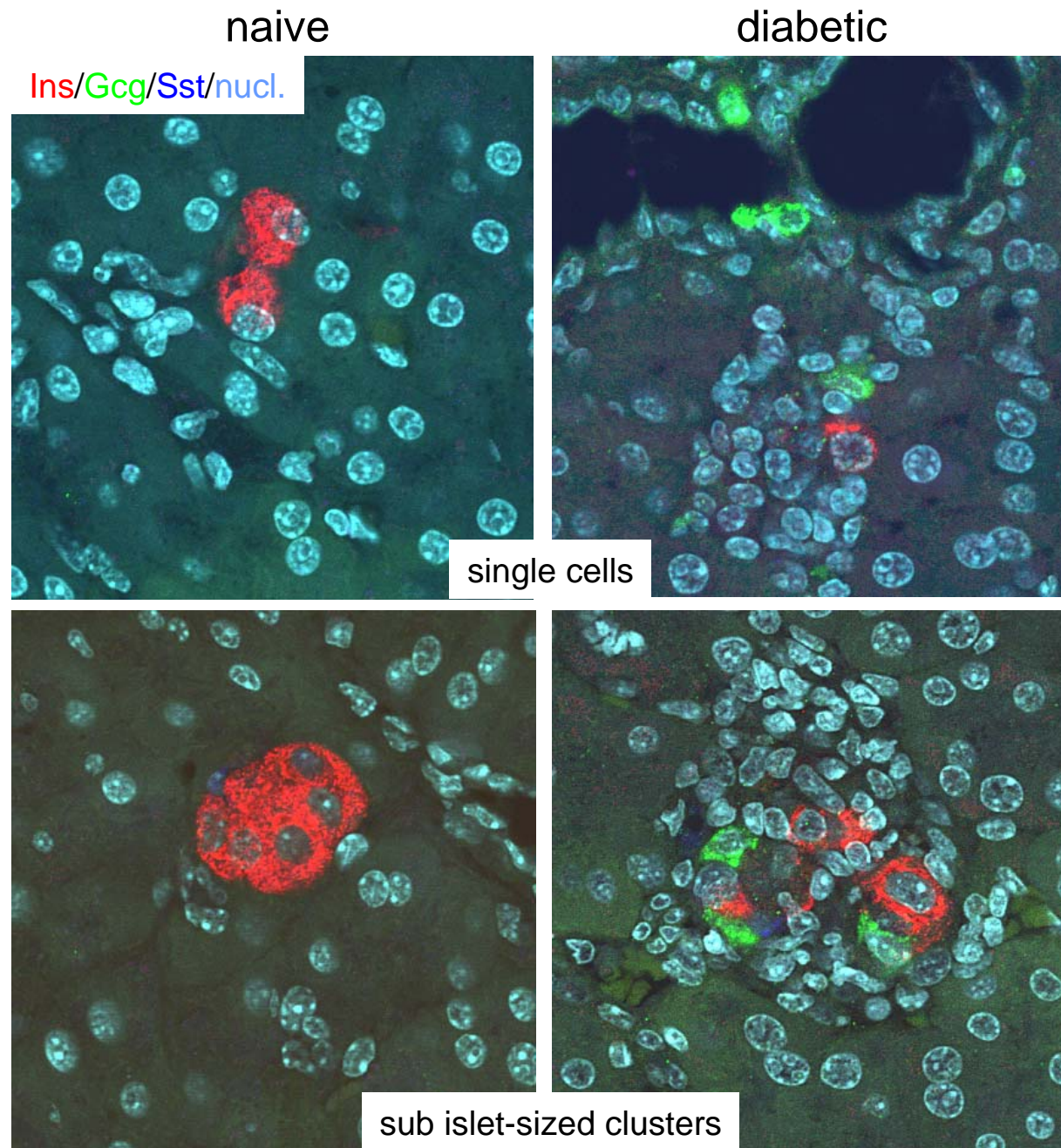
Online Appendix Figure 2: Islet size-dependent alterations in insulin+/glucagon+ endocrine cell content. Pancreatic sections from naïve (n=3, open symbols) and newly diabetic mice (n=5, black) were examined by immunofluorescence. Endocrine cell numbers of individual islet cross-sections were scored and the overall endocrine cell count for each islet plotted against the relative frequency of A: insulin+ or B: glucagon+ cells. Robust regression analysis (cubic polynomial fit), assuming a heteroscedastic distribution of variances and applying Beaton-Tukey weighted outlier analysis was used to describe the islet size versus insulin+ or glucagon+ cell frequencies in immunofluorescence detected islet images of pancreatic sections of naïve (grey lines) and diabetic pancreas (black lines): Ins+ fraction, left: naïve, $R^2 = 0.54$, $p < 0.0001$; diabetic, 0.20 , $p < 0.0001$. Corresponding Gcg+ fraction (right) were: 0.75 , $p < 0.0001$, and 0.19 , $p < 0.0001$, for naïve and diabetic islets, respectively. These results are consistent with increased Ins-to-Gcg ratios, observed by flow cytometry and qRT-PCR using purified, handpicked islets, conceivably containing more of the larger islets.

Online Appendix Figure 3 Pechhold et al.



Online Appendix Figure 3: Abundance of insulin and glucagon mRNA in different anatomic pancreas compartments of naïve and recently diabetic mice. Whole tissue (squares, left panel) represents small biopsy specimen (5-10 mg), purified islets (circles, middle panel), and viable pancreatic tissue depleted of all discernible islets (triangles, right panel) were examined for insulin and glucagon mRNA by qRT-PCR. The insulin-to-glucagon ratio of naïve (grey) and recently diabetic mice (black) was calculated (2^{ddCT}), and plotted using a semi-log scale. Each symbol represents one mouse, and vertical bars indicate the arithmetic means for naïve and diabetic groups of mice. They are: whole tissue: 12.3, 3.4; islets: 2.9, 4.9; islet-depleted cells: 31.0, 9.6). P-values were 0.17 (islets), and 0.016 (*, islet-depleted tissue), respectively. Note that the reduction of insulin-to-glucagon ratios found outside existing islets and overall in the pancreas was not paralleled in purified islets.

Online Appendix Figure 4 Pechhold et al.



Supplementary Figure 4: Small, endocrine cell clusters reveal a distinctive composition at diabetes onset. Insulin expression is by far the most dominant hormone detected in scattered cells or small clusters outside established islets of naïve mice. 80% (40/50) of clusters comprising ≤ 5 endocrine islet cells each express insulin but not glucagon or somatostatin (left panel, single cells – top, small clusters – bottom). In contrast, diabetic pancreata display a distinct small cluster composition: only 11/23 (48%) expressed insulin alone, and marked immune cell infiltrates virtually always were found in the vicinity of insulin+ but not insulin-negative HSIC clusters (right panel, single cells – top, small clusters – bottom). These findings indicate a profound distortion of endocrine cell composition in diabetic pancreata, and suggest that the presence of immune cells outside the confines of traditionally recognized islets reflect the presence of antigenic, scattered beta cells.